Suppression of aerodynamic response of suspension bridges during erection and after completion by using tuned mass dampers

Virote Boonyapinyo[†]

Department of Civil Engineering, Thammasat University, Rangsit Campus, Pathumthani 12120, Thailand

Adul Aksorn[‡]

Faculty of Architecture, Khon Kean University, Khon Kean 40002, Thailand

Panitan Lukkunaprasit[‡†]

Department of Civil Engineering, Chulalongkorn University, Bangkok 10330, Thailand

Abstract. The suppression of aerodynamic response of long-span suspension bridges during erection and after completion by using single TMD and multi TMD is presented in this paper. An advanced finite-element-based aerodynamic model that can be used to analyze both flutter instability and buffeting response in the time domain is also proposed. The frequency-dependent flutter derivatives are transferred into a time-dependent rational function, through which the coupling effects of three-dimensional aerodynamic motions under gusty winds can be accurately considered. The modal damping of a structure-TMD system is analyzed by the state-space approach. The numerical examples are performed on the Akashi Kaikyo Bridge with a main span of 1990 m. The bridge is idealized by a three-dimensional finite-element model consisting of 681 nodes. The results show that when the wind velocity is low, about 20 m/s, the multi TMD type 1 (the vertical and horizontal TMD with 1% mass ratio in each direction together with the torsional TMD with ratio of 1% mass moment of inertia) can significantly reduce the buffeting response in vertical, horizontal and torsional directions by 8.6-13%. When the wind velocity increases to 40 m/s, the control efficiency of a multi TMD in reducing the torsional buffeting response increases greatly to 28%. However, its control efficiency in the vertical and horizontal directions reduces. The results also indicate that the critical wind velocity for flutter instability during erection is significantly lower than that of the completed bridge. By pylon-to-midspan configuration, the minimum critical wind velocity of 57.70 m/s occurs at stage of 85% deck completion.

Keywords: aerodynamic response; suspension bridges; Akashi Kaikyo Bridge; tuned mass dampers.

† Associate Professor, Corresponding Author, E-mail: bvirote@engr.tu.ac.th
‡ Lecturer
‡† Professor

1. Introduction

Wind-induced flutter instability and buffeting response are particularly important aerodynamic responses of long-span suspension bridges and long-span cable-stayed bridges. The wind effect must be taken into account not only for the completed bridge but also for the bridge during erection. Flutter is a phenomenon of self-excited vibration, which may cause a bridge to vibrate continuously with increasing amplitude until the bridge structure fails. A large buffeting amplitude may cause fatigue damage in structural members or make drivers and passengers in moving vehicles feel uncomfortable. With the rapid increase in the span length of modern cable-stayed and suspension bridges, research on aerodynamic response analysis and its suppression of long-span bridges during erection and after completion has become a problem of great concern.

Although the period of deck erection is usually not too long and the expected wind velocity for this period can be reduced accordingly, the overall stiffness of the bridge during erection is significantly less compared to that of the completed bridge in service condition. Therefore, the general conditions against the aerodynamic instability are found to be less favorable than the completed bridge (Brancaleoni 1992, Tanaka, *et al*. 1998, Ge and Tanaka 2000, Cobo del Arco 2001). For truss stiffened bridges, the problem may be solved by erecting the open truss first (Larsen and Gimsing 1992) but this can not be done in box-girder suspension bridges. The suppression of aerodynamic response of long-span suspension bridges during erection and after completion can be done by the control method and the choice of erection method.

The strategy for the control of wind-induced vibration of long-span bridges can be classified as structural countermeasures, aerodynamic countermeasures and mechanical countermeasures. The structural countermeasures are done by increasing the first torsional frequency and the ratio between the first symmetric torsional and vertical bending frequencies. This method can obviously improve the flutter behavior of bridges (Simiu and Scanlan 1996). The aerodynamic countermeasures are usually an effective method for response suppression. Wardlaw (1992) summarized the countermeasures for improving the aerodynamic stability of bridge decks and noted that a satisfying aerodynamic performance of bridge decks can be achieved by the use of shallow sections, closed sections, edge streamlining and other minor or subtle changes to the cross-section geometry. Active aerodynamic countermeasures have also been studied for increasing the critical flutter wind speed (Wilde and Fujino 1998).

Past and present researches on the mechanical countermeasure of the buffeting response (Malhortra and Wieland 1987, Miyata, *et al*. 1993, Conti, *et al*. 1996, Gu, *et al*. 2001, Chang, *et al*. 2003) and flutter response (Nobuto, *et al*. 1988, Gu, *et al*. 1998, Pourzeynali and Datta 2002, Kwon and Park 2004) of long-span bridges focus mainly on the tuned mass damper (TMD). Conti, *et al*. (1996) showed that the TMD can reduce the horizontal buffeting response in terms of standard derivative value by 35% in a full aeroelastic model test of the Normandie cable-stayed bridge during erection. However, previous researches on the suppression of aerodynamic response of long-span bridges are generally based on: (1) the spectral approach which uses only two modes, that is, the first vertical mode and the first torsional mode, with the results being limited to the buffeting response only in terms of the standard derivative values; and (2) the simplified aerodynamic model that does not consider the combined flutter instability and buffeting response and neglects the aeroelastic coupling between modes. Boonyapinyo, *et al*. (1999) and Chen, *et al*. (2000a) showed that neglecting the effects of aeroelastic coupling between modes results in a significant underestimation of the torsional displacement response and produces a considerable difference in the

vertical response at high wind velocities.

In addition, previous research on multi-mode coupled flutter analysis and its suppression are commonly performed through the solution of a nonlinear complex eigenvalue problem (Miyata and Yamada 1988, Agar 1991). Since unsteady self-excited forces are a function of reduced frequency, each solution associated with each mode needs an iterative calculation until the assumed frequency coincides with that of the prescribed target mode. This procedure can be time consuming and computationally cumbersome particularly for the multi-mode flutter analysis of long span bridges that have closely-spaced frequencies. Recently, the computational efficiency of flutter analysis has been improved by representing the unsteady self-excited forces in terms of a rational function approximation (Fujino, *et al.* 1995, Boonyapinyo, *et al.* 1999, Chen, *et al.* 2000a, 2000b). Accordingly, the multi-mode coupled flutter analysis is reduced to evaluate the eigenvalues of a constant matrix at each prescribed wind velocity. Very few researches, if any, on the suppression of aerodynamic response of long-span suspension bridges by using TMD have been based on an advanced aerodynamic model that considers combined flutter instability and buffeting response in time domain and aeroelastic coupling between modes. An accurate estimation of the suppression of aerodynamic response requires a precise prediction of the aerodynamic damping and proper consideration of the changes that take place in mode shapes due to aerodynamic coupling. With the rapid increase in the span length of modern cable-stayed and suspension bridges, an advanced finite-element-based aerodynamic model must be considered and then the control efficiency of TMD with wind velocity could be better understood and accurately investigated.

In this paper, the suppression of aerodynamic response of long-span suspension bridges during erection and after completion by using single TMD and multi TMD is presented. An advanced finite-element-based aerodynamic model that can be used to analyze both flutter instability and buffeting response in the time domain is also proposed. The equation of motion in the time domain is expressed in modal-coordinate state-space form. The frequency-dependent flutter derivatives are transferred into a time-dependent rational function, through which the coupling effects of three-dimensional aerodynamic motions under gusty winds can be accurately considered. The buffeting forces are considered through a quasi-steady formulation together with the appropriate aerodynamic admittances. The modal damping of a structure-TMD system is analyzed by the state-space approach. The numerical examples are performed on the Akashi Kaikyo Bridge with a main span of 1990 m during erection and after completion by using single TMD and multi TMD.

2. Turbulent wind model and its simulation

The turbulent wind model consists of a steady part (related to mean wind speed) and a superimposed fluctuating part. The fluctuating wind forces acting on the structure depend on the size of gust in relation to the size of the structure. This dependence can be expressed in terms of the aerodynamic admittance, which is a ratio of the fluctuating force in the turbulent wind to the quasi-static force in the steady flow. The multidimensional autoregressive moving average (ARMA) proposed by Samaras, *et al.* (1985) for generating the time-space correlated fluctuating wind velocity along the bridge is applied. The details of the turbulent wind model are given by Miyata, *et al.* (1995), among others.

3. Aerodynamic force model and equation of motion

The aerodynamic force model is assumed to consist of: (1) frequency-dependent aeroelastic force

due to wind-structure interaction in a smooth on coming wind flow; and (2) time-and-space-dependent buffeting force due to turbulence in an oncoming wind flow, but neglected interactive with structural motion. Then, the sectional aerodynamic wind forces per unit span are defined as

$$\text{Lift: } L = L_{ae} + L_b \tag{1a}$$

$$\text{Drag: } D = D_{ae} + D_b \tag{1b}$$

$$\text{Moment: } M = M_{ae} + M_b \tag{1c}$$

where subscript *ae* refers to aeroelastic effects; and *b* to buffeting effects.

The quasi-steady buffeting lift, drag and moment forces are expressed in terms of steady average (or static) lift, drag and moment force coefficients C_L, C_D and C_M, respectively, (Simiu and Scanlan 1996) as

$$L_b = \frac{1}{2}\rho U^2 B\left[C_L\left(1 + 2\frac{u}{U}\right) + \left(C_L' + \frac{A_n}{B}C_D\right)\frac{w}{U}\right] \tag{2a}$$

$$D_b = \frac{1}{2}\rho U^2 A_n\left[C_D\left(1 + 2\frac{u}{U}\right) + C_D'\frac{w}{U}\right] \tag{2b}$$

$$M_b = \frac{1}{2}\rho U^2 B^2\left[C_M\left(1 + 2\frac{u}{U}\right) + C_M'\frac{w}{U}\right] \tag{2c}$$

where U=mean along-wind velocity; ρ=air density; B=deck width; $u=u(t)$ and $w=w(t)$ are the horizontal and vertical gust (or fluctuation) velocity components of the wind; A_n=projected area of the deck normal to the wind direction; $C_L' = dC_L/d_\alpha$; $C_D' = dC_D/d_\alpha$; $C_M' = dC_M/d_\alpha$; α=wind angle of attack.

Because the aeroelastic forces depend on reduced frequency while the buffeting forces naturally depend on time and spatial location, the frequency-dependent aeroelastic forces are transformed into the time-dependent forces so that they can be applied in an explicit time-domain approach. The most common form of the approximation of aeroelastic force coefficients used currently in aeronautics is a rational function of the nondimentional Laplace variable p where $p=sB/U=iK$ and nondimensional time $s=Ut/B$.

Thus, for sinusoidal motion in the vertical y, rotation q, and horizontal z directions, the linearlized forms of the aeroelastic or self-excited forces are completely expressed in the Laplace domain as

$$\left\{\begin{matrix}\bar{L}_{ae} \\ \bar{D}_{ae} \\ \bar{M}_{ae}\end{matrix}\right\} = \frac{1}{2}\rho U^2\begin{bmatrix}B & & \\ & B & \\ & & B^2\end{bmatrix}\begin{bmatrix}K^2 H_1^*i + K^2 H_4^* & K^2 H_5^*i + K^2 H_6^* & K^2 H_2^*i + K^2 H_3^* \\ K^2 P_5^*i + K^2 P_6^* & K^2 P_1^*i + K^2 P_4^* & K^2 P_2^*i + K^2 P_3^* \\ K^2 A_1^*i + K^2 A_4^* & K^2 A_5^*i + K^2 A_6^* & K^2 A_2^*i + K^2 A_3^*\end{bmatrix}\left\{\begin{matrix}\bar{y}/B \\ \bar{z}/B \\ \bar{\theta}_x\end{matrix}\right\} \tag{3}$$

where the aeroelastic coefficients matrix can be expressed in the rational function or partial fraction form (Boonyapinyo, *et al.* 1999); $K=B\omega/U$=reduced frequency; ω=natural frequency; and H_i^*, P_i^*, A_i^*, $(i=1-6)$=experimentally obtained flutter derivatives or aeroelastic coefficients.

Finally, the equation of motion in the time domain is expressed with a modal-coordinated state-space form as (Boonyapinyo, *et al.* 1999)

$$
\begin{Bmatrix} \dot{\mathbf{q}} \\ \ddot{\mathbf{q}} \\ \dot{\mathbf{x}}_3 \\ \vdots \\ \dot{\mathbf{x}}_{m+2} \end{Bmatrix} =
\begin{bmatrix}
\mathbf{0} & \mathbf{I} & \mathbf{0} & \cdots & \mathbf{0} \\
-\hat{\mathbf{M}}^{-1}\hat{\mathbf{K}} & -\hat{\mathbf{M}}^{-1}\hat{\mathbf{C}} & \frac{1}{2}\rho U^2 \hat{\mathbf{M}}^{-1} & \cdots & \frac{1}{2}\rho U^2 \hat{\mathbf{M}}^{-1} \\
\mathbf{0} & \mathbf{A}_3 & -\frac{U}{B}b_3\mathbf{I} & \cdots & \mathbf{0} \\
\vdots & \vdots & \vdots & \ddots & \vdots \\
\mathbf{0} & \mathbf{A}_{m+2} & \mathbf{0} & \cdots & -\frac{U}{B}b_{m+2}\mathbf{I}
\end{bmatrix}
\begin{Bmatrix} \mathbf{q} \\ \dot{\mathbf{q}} \\ \mathbf{x}_3 \\ \vdots \\ \mathbf{x}_{m+2} \end{Bmatrix} +
\begin{Bmatrix} \mathbf{0} \\ \hat{\mathbf{M}}^{-1} \\ \mathbf{0} \\ \vdots \\ \mathbf{0} \end{Bmatrix} \mathbf{F}_b
\qquad (4)
$$

or symbolically expressed as

$$
\dot{\eta}(t) = \mathbf{A}\,\eta(t) + \mathbf{B}\,\mathbf{F}_b(t) \qquad (5)
$$

where $\hat{\mathbf{M}} = \mathbf{M} - \frac{1}{2}\rho B^2 \mathbf{A}_2$; $\hat{\mathbf{C}} = \mathbf{C} - \frac{1}{2}\rho UB \mathbf{A}_1$; $\hat{\mathbf{K}} = \mathbf{K} - \frac{1}{2}\rho U^2 \mathbf{A}_0$; modal aeroelastic matrix $\mathbf{A}_l = \Phi^{t}\mathbf{a}_l\Phi$, $l = 0, 1, 2, ..., m+2$; Φ = natural mode shape; $\mathbf{a}_l$ = aeroelastic matrix in the form of rational function approximation; $\mathbf{M}$, $\mathbf{C}$ and $\mathbf{K}$ = modal mass, damping, and stiffness matrices, respectively; $\hat{\mathbf{M}}, \hat{\mathbf{C}}$, and $\hat{\mathbf{K}}$ = aeroelastic-modified modal mass, damping, and stiffness matrices, respectively; $\mathbf{x}_l$, $l = 3, 4, ..., m+2$, = aerodynamic state vectors; U = mean along-wind velocity; $\mathbf{q}$ = generalized coordinate; $\mathbf{F}_b$ = modal buffeting force vector; m = partial fraction or lag terms for the approximation of flutter derivatives generally varied from 2 to 4 depending on their characteristics.

Because Eq. (4) explicitly includes both aeroelastic and buffeting forces, it can be used to analyze: (1) several types of aerodynamic instability, such as, galloping, torsional flutter, and flexural-torsional flutter; and (2) combined flutter instability and buffeting responses. Details of the solution of flutter velocity under smooth wind and the solution of buffeting response under turbulent wind are given by Boonyapinyo, *et al.* (1999).

4. Design of tuned mass dampers

4.1. Equation of motion of structure-TMD system

The modeling of the bridge-TMD system and TMD at the span-center for horizontal, vertical and torsional directions is shown in Fig. 1. The equation of motion for a multi-degree-of-freedom system with a TMD 1 and a TMD 2 attached to h^{th} and k^{th} degrees of freedom, respectively, subjected to wind load $\mathbf{p}$ is given by:

$$
\mathbf{m}\ddot{\mathbf{u}} + \mathbf{c}\dot{\mathbf{u}} + \mathbf{k}\mathbf{u} = \mathbf{p} \qquad (6)
$$

The solution can be expressed by the modal analysis as

$$
\mathbf{u} = \begin{Bmatrix} \mathbf{u}_s \\ u_{t1} \\ u_{t2} \end{Bmatrix} = \mathbf{A}\mathbf{x} =
\begin{bmatrix}
\varphi_1 & \cdots & \varphi_n & \mathbf{0} & \mathbf{0} \\
0 & \cdots & 0 & 1 & 0 \\
0 & \cdots & 0 & 0 & 1
\end{bmatrix}
\begin{Bmatrix} \mathbf{x}_s \\ x_{t1} \\ x_{t2} \end{Bmatrix} \qquad (7)
$$

where $\mathbf{u}_s$ = vector of absolute displacement of the main structure; u_{t1} and u_{t2} = absolute displacements of TMD 1 and TMD 2, respectively; $\mathbf{x}_s$ = vector of generalized-coordinate displacement of main structure;
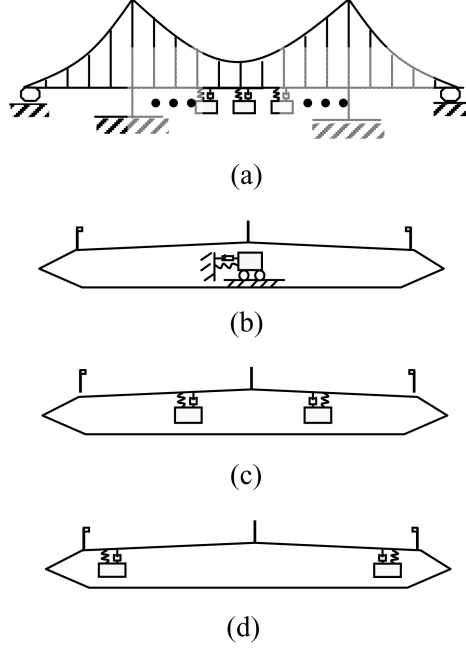
(a)

(b)

(c)

(d)

Fig. 1 (a) Modeling of bridge-TMD system; and TMD at the span-center section for: (b) horizontal; (c) vertical; (d) torsional directions

x_{t1} and x_{t2} = generalized-coordinate displacements of TMD 1 and TMD 2, respectively; $\varphi_n = n^{\text{th}}$ natural mode shape of the main structure without TMD, normalizing such that modal mass=1.

By substituting Eq. (7) into Eq. (6) and premultiplying Eq. (6) with the transpose of **A**, the equation of motion in modal coordinates can be written as

$$\mathbf{M}\ddot{\mathbf{x}} + \mathbf{C}\dot{\mathbf{x}} + \mathbf{K}\mathbf{x} = \mathbf{P} \tag{8}$$

where

$$\mathbf{M} = \text{diag}(1, 1, ..., 1_n, m_{t1}, m_{t2}) \tag{9}$$

$$\mathbf{C} = \mathbf{A}^T\mathbf{c}\mathbf{A} = \begin{bmatrix} \varphi_1^T\mathbf{c}_s\varphi_1 & \cdots & 0 & 0 & 0 \\ \vdots & \ddots & \vdots & \vdots & \vdots \\ 0 & \cdots & \varphi_n^T\mathbf{c}_s\varphi_n & 0 & 0 \\ 0 & \cdots & 0 & 0 & 0 \\ 0 & \cdots & 0 & 0 & 0 \end{bmatrix} + c_{t1}\begin{bmatrix} \phi_{1h}\phi_{1h} & \cdots & \phi_{1h}\phi_{nh} & -\phi_{1h} & 0 \\ \vdots & \ddots & \vdots & \vdots & \vdots \\ \phi_{nh}\phi_{1h} & \cdots & \phi_{nh}\phi_{nh} & -\phi_{nh} & 0 \\ -\phi_{1h} & \cdots & -\phi_{nh} & 1 & 0 \\ 0 & \cdots & 0 & 0 & 0 \end{bmatrix} + c_{t2}\begin{bmatrix} \phi_{1k}\phi_{1k} & \cdots & \phi_{1k}\phi_{nk} & 0 & -\phi_{1k} \\ \vdots & \ddots & \vdots & \vdots & \vdots \\ \phi_{nk}\phi_{1k} & \cdots & \phi_{nk}\phi_{nk} & 0 & -\phi_{nk} \\ 0 & \cdots & 0 & 0 & 0 \\ -\phi_{1k} & \cdots & -\phi_{nk} & 0 & 1 \end{bmatrix} \tag{10}$$

$$\mathbf{K} = \mathbf{A}^T\mathbf{k}\mathbf{A} = \begin{bmatrix} \varphi_1^T\mathbf{k}_s\varphi_1 & \cdots & 0 & 0 & 0 \\ \vdots & \ddots & \vdots & \vdots & \vdots \\ 0 & \cdots & \varphi_n^T\mathbf{k}_s\varphi_n & 0 & 0 \\ 0 & \cdots & 0 & 0 & 0 \\ 0 & \cdots & 0 & 0 & 0 \end{bmatrix} + k_{t1}\begin{bmatrix} \phi_{1h}\phi_{1h} & \cdots & \phi_{1h}\phi_{nh} & -\phi_{1h} & 0 \\ \vdots & \ddots & \vdots & \vdots & \vdots \\ \phi_{nh}\phi_{1h} & \cdots & \phi_{nh}\phi_{nh} & -\phi_{nh} & 0 \\ -\phi_{1h} & \cdots & -\phi_{nh} & 1 & 0 \\ 0 & \cdots & 0 & 0 & 0 \end{bmatrix} + k_{t2}\begin{bmatrix} \phi_{1k}\phi_{1k} & \cdots & \phi_{1k}\phi_{nk} & 0 & -\phi_{1k} \\ \vdots & \ddots & \vdots & \vdots & \vdots \\ \phi_{nk}\phi_{1k} & \cdots & \phi_{nk}\phi_{nk} & 0 & -\phi_{nk} \\ 0 & \cdots & 0 & 0 & 0 \\ -\phi_{1k} & \cdots & -\phi_{nk} & 0 & 1 \end{bmatrix} \tag{11}$$

$$\mathbf{P} = \mathbf{A}^T\mathbf{p} = \begin{Bmatrix} \boldsymbol{\varphi}_1^T\mathbf{p} \\ \vdots \\ \boldsymbol{\varphi}_n^T\mathbf{p} \\ 0 \\ 0 \end{Bmatrix} \tag{12}$$

and m_{t1}, c_{t1}, and k_{t1} = mass, damping coefficient, and stiffness of TMD 1; m_{t2}, c_{t2}, and k_{t2} = mass, damping coefficient, and stiffness of TMD 2.

Finally, the modal damping of the structure-TMD system can be analyzed by the state-space approach.

4.2. Optimal damping ratio of TMD

To simplify the analysis by neglecting the structural damping ratio, the optimal damping ratio of TMD ($\xi_{t, opt}$) and tuned parameter ($f_{t, opt} = \omega_t/\omega_s$) can be obtained for the randomly forced vibration as (Ayorinde and Warburton 1980)

$$\xi_{t, opt} = \sqrt{\frac{\mu(3\mu + 4)}{8(\mu + 1)(\mu + 2)}} \tag{13}$$

$$f_{t, opt} = \sqrt{\frac{\mu + 2}{2(\mu + 1)^2}} \tag{14}$$

where mass ratio $\mu = m_t/m_s$ = the ratio of the TMD mass to the modal mass of structure. For examples, when $\mu = 1\%$ and $\mu = 3\%$, $\xi_{t, opt} = 5\%$ and 8.6%, respectively. The above formula for optimal damping ratio of TMD or similar one was used by many researchers, such as for control of buffeting response (Chang, *et al.* 2003) and for flutter response (Kwon and Park 2004). Gu, *et al.* (1998) were also used similar formula for parametric study on control of flutter response by theoretical and experiment studies. More details of optimal damping ratio of TMD are given by Simiu and Scanlan (1996), among others.

5. Numerical examples of the completed bridge

The flutter and buffeting responses of the Akashi Kaikyo Bridge with a main span of 1990 m and two side spans of 960 m are investigated with and without tuned mass dampers. The completed bridge is idealized by a three-dimensional finite-element model consisting of 681 nodes, as shown in Fig. 3. The stiffening truss girder, as shown in Fig. 2, has a 35.5 m width, a 14 m depth, a 6.74 m^2 projected area normal to the wind direction (A_n) and an offset distance between the shear and gravity centers of 3 m. The aeroelastic matrix $\mathbf{a}_l$ in the form of rational function approximation given by Boonyapinyo, *et al.* (1999) is calculated from experimentally obtained flutter derivatives of stiffening truss girder (modified section) given by the Honshu-Shikoku Bridge Authority (1995). The static aerodynamic coefficients of truss girder are; $C_D = 1.9873$, $C_L = 0.0182$, $C_M = -0.0046$, $C_D = 0.217$, $C_L = 1.612$, $C_M = 0.381$. The static aerodynamic drag coefficients of the main cable and
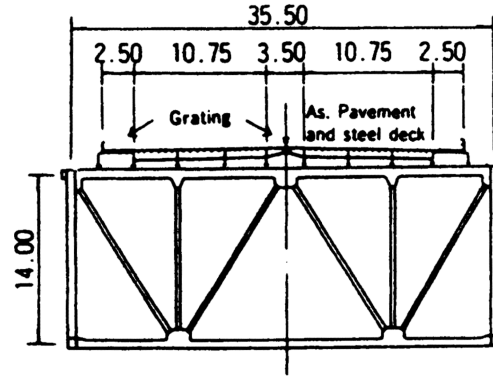
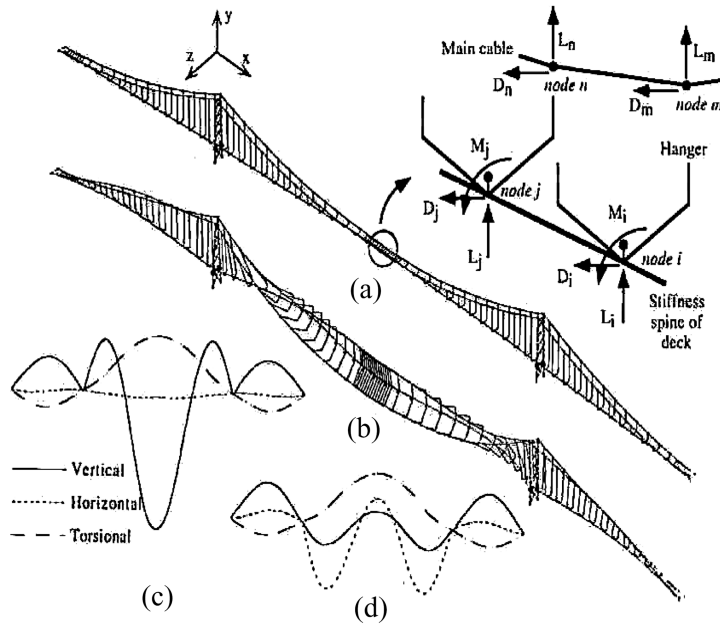Fig. 2 Cross section of a stiffening truss girder of the Akashi Kaikyo Bridge (dimensions in m)

Fig. 3 (a) 3D finite-element modal; (b) 3D flutter mode shape (real part); (c) flutter mode shape of imaginary part; (d) flutter mode shape of real part

tower are 0.7 and 1.8, respectively. In the analysis, the following parameters are used: (1) modal logarithmic decrement $\delta = 0.03$ for horizontal, vertical, and torsional modes; (2) time step increments $= 0.5$ s; (3) winds are generated every 0.5 s; (4) longitudinal turbulence intensity $I_u = 10\%$; vertical turbulence intensity $I_w = I_u/2$; (5) the turbulent wind (mean and fluctuating wind velocities) is applied to the nodal nodes of the deck, while the smooth wind (the mean wind velocity only) is applied to the nodal nodes of the cables and towers; (6) number of structural modes used $= 20$; and (7) the statistical response values are calculated for 10 minutes starting from the 301st second (avoiding starting transient response) to the 900th second. The major natural frequencies and mode shapes of the bridge are shown in Fig. 4; these modes are among the first 20 modes, except for the
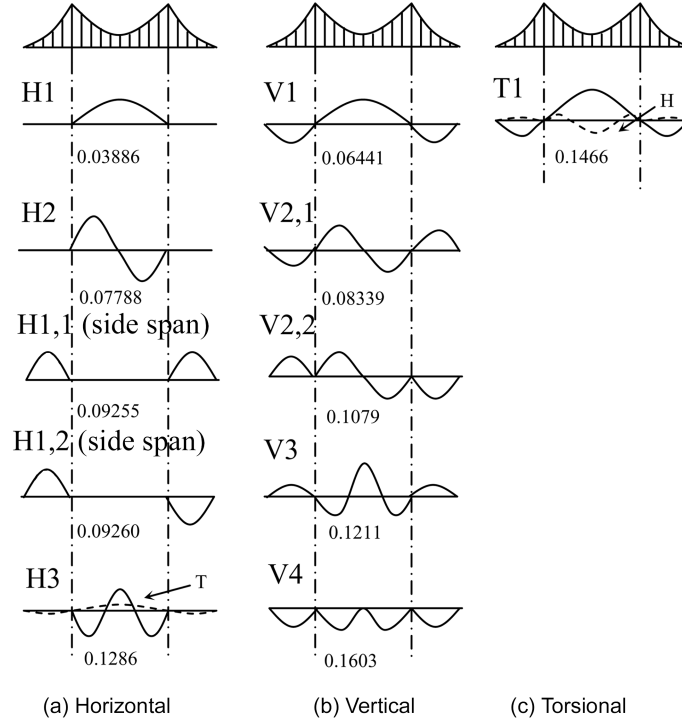
Fig. 4 Natural frequencies (Hz) and modes

second torsional mode (the 23th mode).

Many single TMD in each mode and multi TMD for the suppression of aerodynamic response are investigated in this paper. The optimal damping ratio and frequency of TMD were designed based on Eqs. (13-14). The modal mass of the first vertical, horizontal, and torsional modes of the completed bridge are 6,343 tons, 4,571 tons, and 1,146,542 tons-m^2, respectively. The mass ratio is the ratio of the TMD mass to the modal mass of bridge in each direction.

5.1. Effects of single TMD in each mode on flutter response

Fig. 5 shows the comparisons of critical wind velocities of the completed bridge by using single TMD in each mode with several mass ratios. The results show that the single TMD in each mode results in no significant change in the critical wind velocity for flutter instability. For example, the single TMD that slightly increases the critical wind velocity is as follows: (1) TMD with 1% and 2% mass ratio tuned to V1 mode; (2) TMD with 1% and 2% mass ratio tuned to V3 mode; (3) TMD with 3% and 5% mass moment of inertia tuned to T1 mode. The single TMD that slightly decreases the critical wind velocity is TMD tuned to H1 mode. The single TMD that significantly decreases the critical wind velocity is TMD tuned to H3 mode.

5.2. Effects of multi TMD on flutter response

Many types of multi TMD are investigated. Firstly, the multi TMD type 1 at the span-center
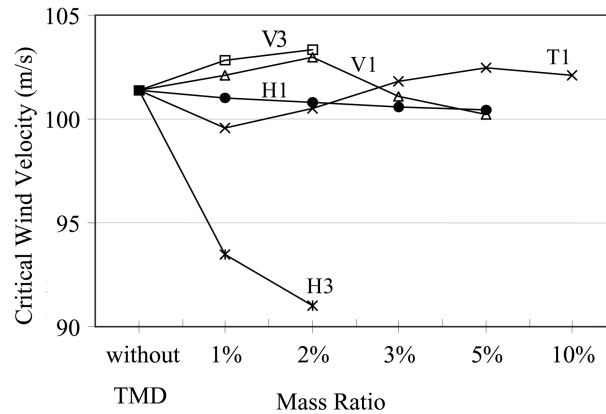
Fig. 5 Comparisons of critical wind velocities of the completed bridge by using TMD in each mode with several mass ratios

section consists of vertical and horizontal TMD with 1% mass ratio in each direction together with torsional TMD with ratio of 1% mass moment of inertia.

For the completed bridge without TMD, the analytical result of a flutter wind velocity of 101.4 m/s is slightly higher than the experimental result of 92.00 m/s obtained from wind-tunnel experiments of the full-bridge aeroelastic model undertaken by the Honshu-Shikoku Bridge Authority (1995). The difference in flutter velocity is probably caused mainly by the flutter derivative as well as the geometric nonlinearity. The flutter derivative may be influenced by the mode shape and displacement amplitude, as discussed by Scanlan (1988), as well as the torsional-displacement-induced wind angle of attack. However, good agreement in flutter mode shape is obtained between the analytical results, as shown in Fig. 3(b-d), and the experimental results. As can be seen in the Fig. 4, the flutter mode shape is coupled among the T1, H3, and V3 modes, which have the natural frequencies close to each other. The horizontal component results mainly from the significant 3 m offset between the shear center and gravity center of the truss girder, as well as the aeroelastic drag forces.

For the completed bridge with multi TMD type 1, the response of system (structural + aerodynamics) frequencies and damping with wind velocity are shown in Figs. 6-7. The analytical result of a flutter wind velocity for the completed bridge with multi TMD type 1 is about 100.1 m/s. The results show that the multi TMD type 1 results in no significant change in the critical wind velocity for flutter instability. This is because the rate of increase of negative aerodynamic damping is so high when the wind velocity approaches the flutter velocity (hard-type flutter), as shown in Fig. 7.

Finally, comparisons of critical wind velocities of the completed bridge by using several multi TMD with several mass ratios in each mode are shown in Fig. 8. Similar to the multi TMD type 1, the results show that the several multi TMDs including the combination of flutter mode H3, V3, and T1 result in no significant change in the critical wind velocity for flutter instability.

5.3. Effects of multi TMD on buffeting response

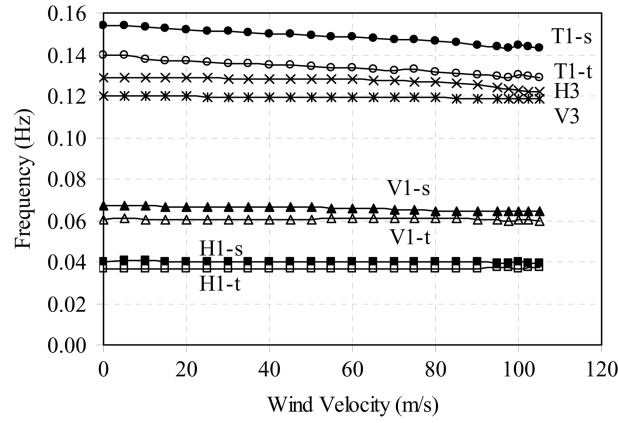The principal concept of multi TMDs is to reduce the dynamic response part in vertical,

Fig. 6 Response of system frequencies with wind velocity for the completed bridge with multi TMD type 1
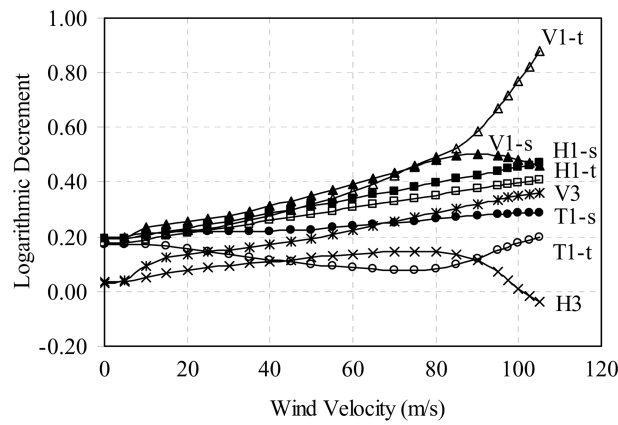

Fig. 7 Response of system damping with wind velocity for the completed bridge with multi TMD type 1
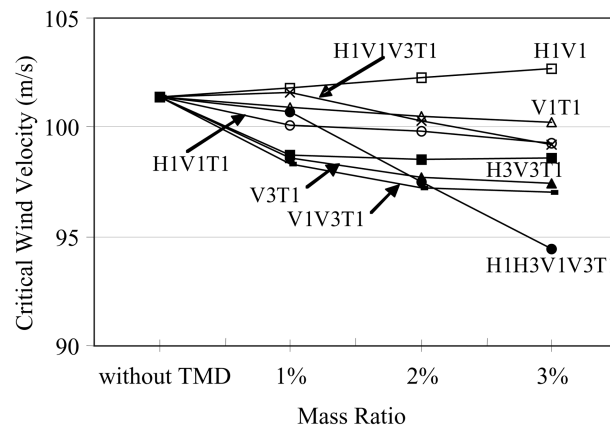

Fig. 8 Comparisons of critical wind velocities of the completed bridge by using several multi TMD with several mass ratios in each mode
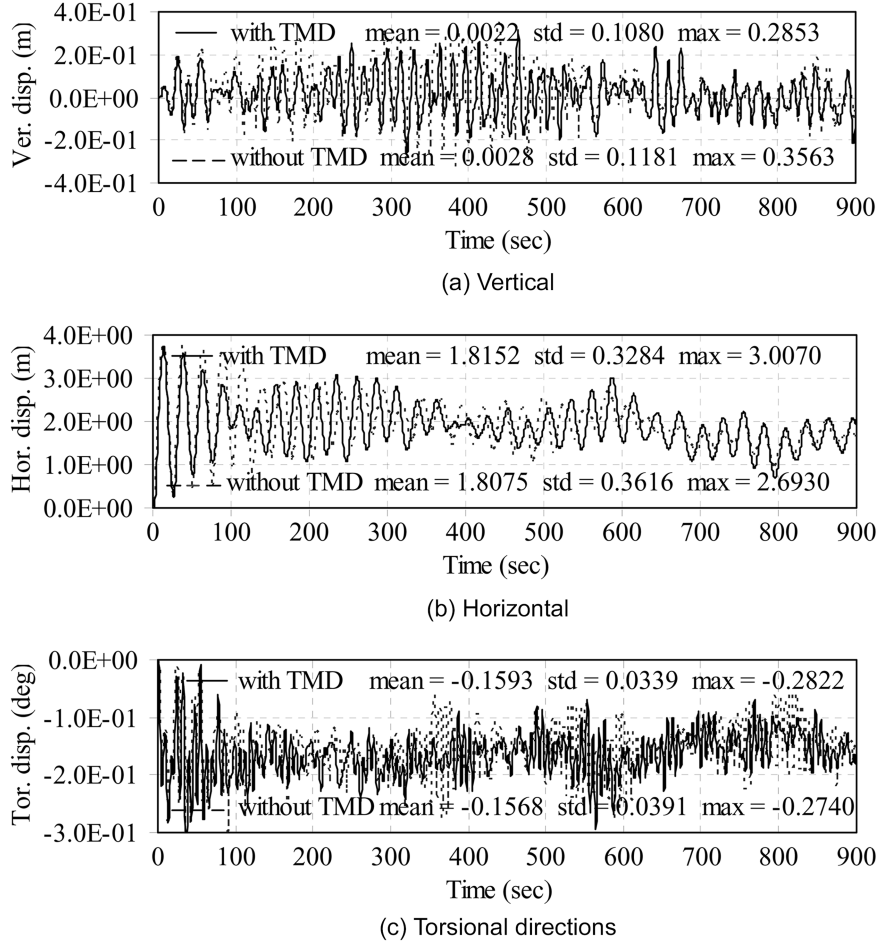
Fig. 9 Displacement response at the center node of the main span for the completed bridge with and without multi TMD type 1 at wind velocity 20 m/s

horizontal and torsional directions, but not the mean (static) response part. Figs. 9 and 10 show comparisons of the displacement response at the center node of the main span with and without multi TMD type 1 at $U=20$ m/s, and 40 m/s, respectively. The results show that when the wind velocity is 20 m/s, the multi TMD type 1 can significantly reduce the buffeting response in terms of the std (standard derivative) values in the vertical, horizontal and torsional directions by 8.6%, 9%, and 13%, respectively. When the wind velocity increases to 40 m/s, the multi TMD type 1 can significantly reduce the torsional buffeting response in term of the std values by 28% [(0.3468-0.2499)/0.3468*100 = 28%], and can moderately reduce the vertical buffeting response by 5.4%. It is noted that when velocity increases, the control efficiency of TMD in reducing the torsional buffeting response increases greatly because the torsional aerodynamic damping reduces with wind velocity (see Fig. 7). However, its control efficiency in vertical and horizontal directions reduces because the aerodynamic dampings in these directions increase with wind velocity (see Fig. 7) and become more dominant than TMD.
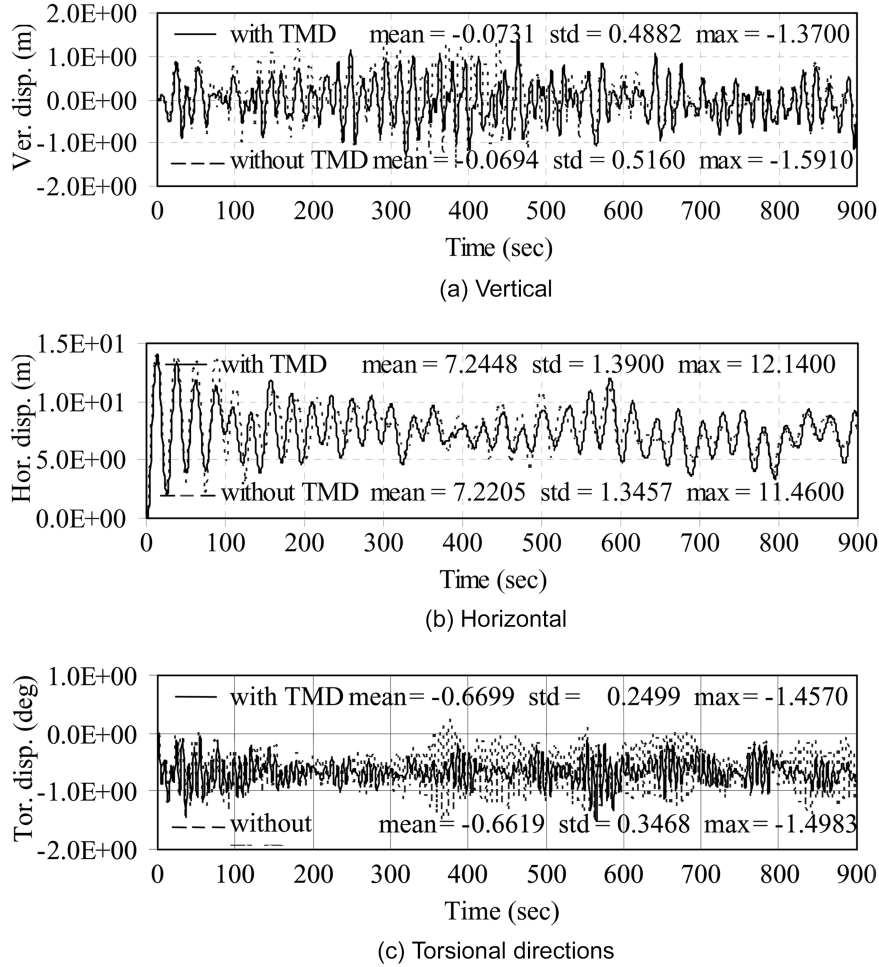
(a) Vertical

(b) Horizontal

(c) Torsional directions

Fig. 10 Displacement response at the center node of the main span for the completed bridge with and without multi TMD type 1 at wind velocity 40 m/s

5.4. Effects of mass ratio of multi TMD on buffeting response and peak stoke

Multi TMD with 1%, 2% and 3% mass ratio tuned to H1 and V1 in each direction and ratio of 1%, 2% and 3% mass moment of inertia tuned to T1 mode are studied. The effects of mass ratio of multi TMD on the std displacement responses at the center node of the main span are shown in Fig. 11. The results show that the control efficiency of TMD in reducing the torsional buffeting response increases greatly as the ratio of mass moment of inertia increase from 1% to 3% at high wind velocity. However, its control efficiency in vertical and horizontal directions tends to saturate or even decrease as the mass ratio increases from 1% to 3%.

The stroke of multi TMD type 1 for the completed bridge at wind velocity 40 m/s is shown in Fig. 12. Because the damper mass absorbs most of the energy of the excitation, its stroke is much larger than that of the bridge (see Figs. 10 and 12). The effects of mass ratio on the peak stroke of
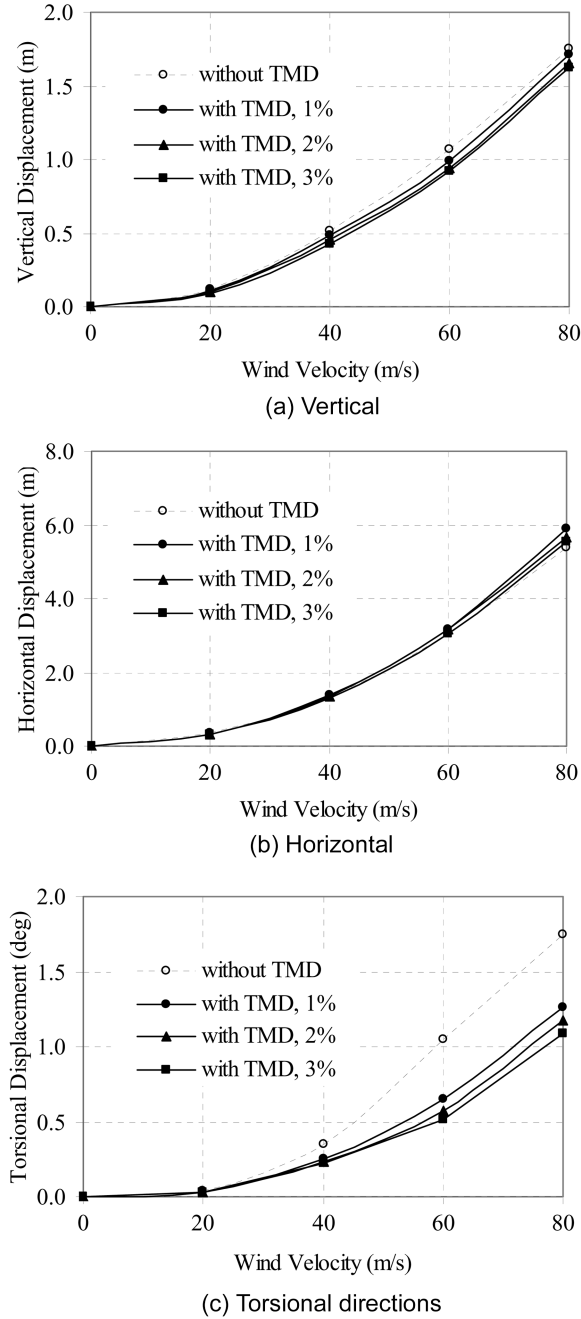
(a) Vertical

(b) Horizontal

(c) Torsional directions

Fig. 11 Effects of mass ratio on std displacement responses at the center node of the main span for the completed bridge with multi TMD tuned to H1, V1 and T1

multi TMD with 1%, 2% and 3% mass ratio tuned to H1 and V1 in each direction and ratio of 1%, 2% and 3% mass moment of inertia tuned to T1 modes at wind velocity 40 m/s are shown in Fig. 13.
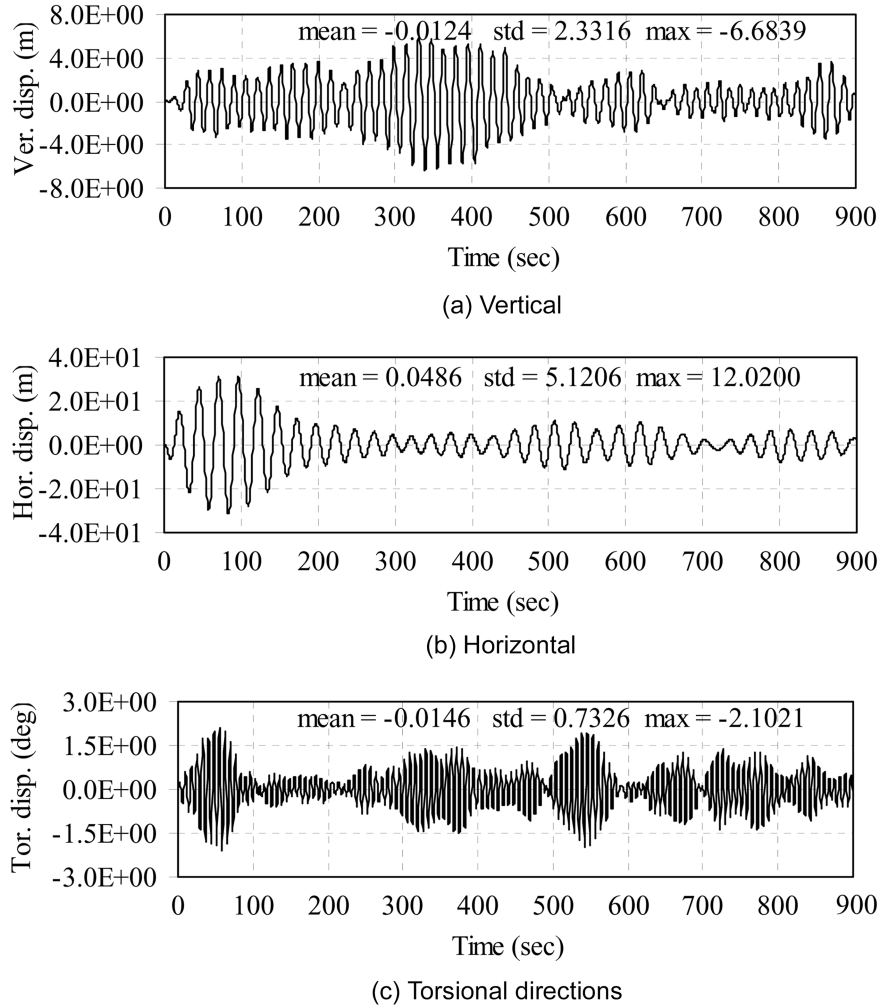
(a) Vertical

(b) Horizontal

(c) Torsional directions

Fig. 12 Stroke of multi TMD type 1 installed at the span-center for the completed bridge at wind velocity 40 m/s

The results show that the peak strokes of TMD in vertical and horizontal directions significantly reduce as the mass ratio increase from 1% to 3%. Therefore, the mass ratio of TMD in vertical and horizontal directions may increase up to 2-3% for a long-span bridge to reduce the peak stroke of TMD and to make its stroke move within the operation range inside the stiffening truss girder.

6. Numerical examples of the bridge during erection

The flutter and buffeting responses of the Akashi Kaikyo Bridge during erection are investigated with and without tuned mass dampers. Deck erection of the suspension bridge involves many challenging problems with respect to both construction safety and time schedules. It needs to be carefully selected by considering all practical aspects, such as geometry control, static and dynamic stress, as well as the aerostatic and aerodynamic stabilities. In this research, two typical types of
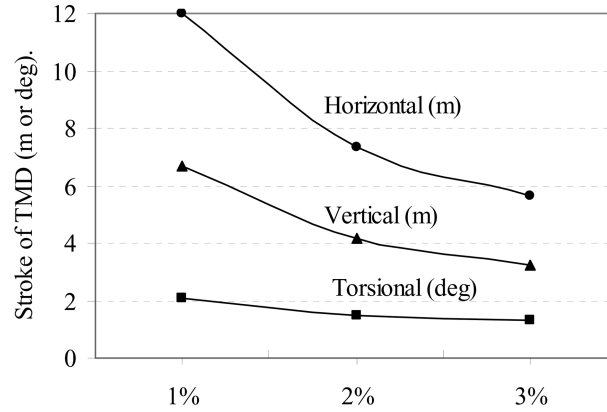
Fig. 13 Effect of mass ratio on the peak stroke of multi TMD type 1 for the completed bridge at wind
     velocity of 40 m/s

(a) Midspan-to-pylon configuration   (b) Pylon-to-midspan configuration

Fig. 14 Deck erection sequence

deck erection sequence (Gimsing 1997) shown in Fig. 14 are investigated as follows: (1) midspan-
to-pylon configuration, and (2) pylon-to-midspan configuration.

6.1. Natural frequencies of the bridge during erection

The natural frequencies of the bridge during erection by midspan-to-pylon and pylon-to-midspan
are shown in Figs. 15 and 16, respectively. Some important results can be summarized as follows.
(1) The first horizontal frequency is not influenced significantly by the percentage of the erected
deck length nor the erection sequence. This implies that the ratio of the effective stiffness to the
effective mass in the first horizontal mode remains more or less at the same value. (2) The first
vertical frequency and the first torsional frequency by the pylon-to-midspan configuration are higher
than those by the midspan-to-pylon configuration. This means that the pylon-to-midspan
configuration is stiffer than the midspan-to-pylon configuration. (3) The third horizontal frequency
is influenced significantly by the percentage of the erected deck length and the erection sequence.

6.2. Flutter response of the bridge during erection

The critical wind velocities for flutter during erection between midspan-to-pylon configuration and
pylon-to-midspan configuration are compared in Fig. 17. Some important results can be summarized
as follows. (1) The critical wind velocity during erection is significantly lower than that of the
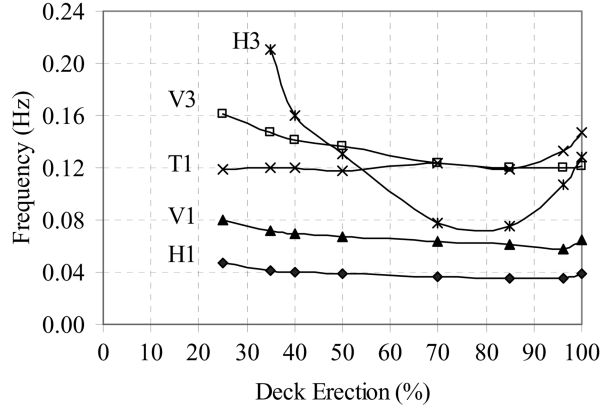completed bridge, especially at the stage of 25-95% deck completion by midspan-to-pylon

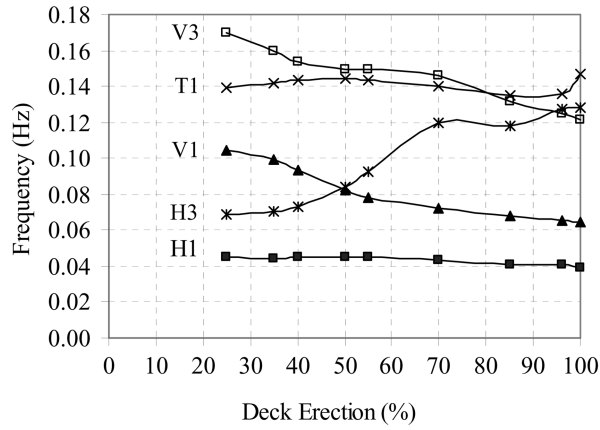Fig. 15 Comparisons of natural frequencies during erection by midspan-to-pylon configuration

Fig. 16 Comparisons of natural frequencies during erection by pylon-to-midspan configuration

configuration and at stage of 55-95% deck completion by pylon-to-midspan configuration. (2) The critical wind velocity during erection by pylon-to-midspan configuration is significantly higher than that by midspan-to-pylon configuration. (3) By midspan-to-pylon configuration, the first minimum critical wind velocity of 41.20 m/s occurs at an early stage of about 25-40% deck completion, and the second minimum critical wind velocity of 45.70 m/s occurs at the stage of 85% deck completion. (4) By pylon-to-midspan configuration, the minimum critical wind velocity of 57.70 m/s occurs at the stage of 85% deck completion. At this stage, the contribution of the deck to the overall stiffness is not yet fully developed and the bridge deck is very long to pick up the aerodynamic forces, together with the natural frequencies of T1, V3, and H3 modes that cause flutter and which are close to each other.

The flutter mode shapes in real part at 85% deck completion by midspan-to-pylon configuration and by pylon-to-midspan configuration are shown in Figs. 18 and 19, respectively. As can be seen in the figures, similar to the completed bridge, the flutter mode shapes in two types of erection sequence are still coupled among the T1, H3, and V3 modes.
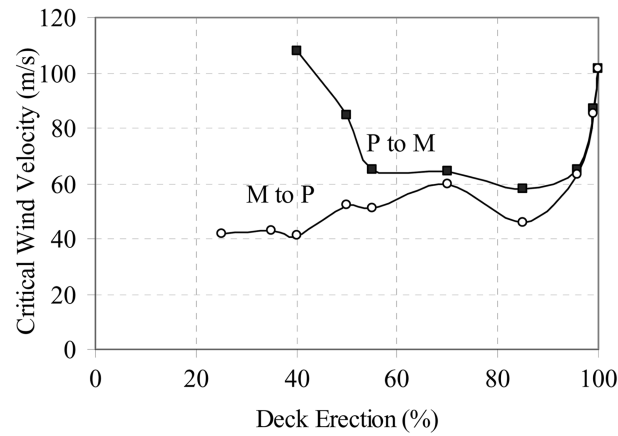
Fig. 17 Comparisons of critical wind velocities during erection by midspan-to-pylon and pylon-to-midspan
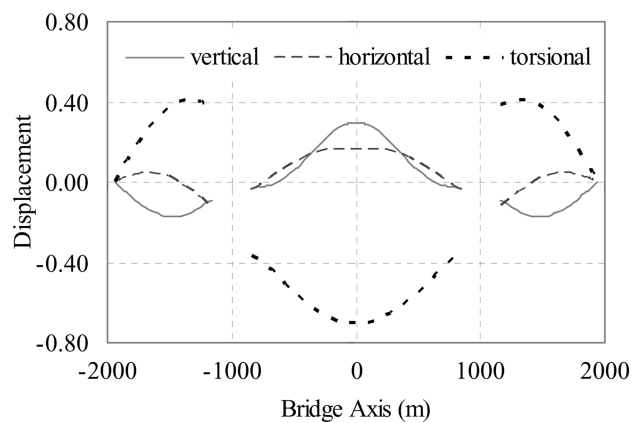   configurations

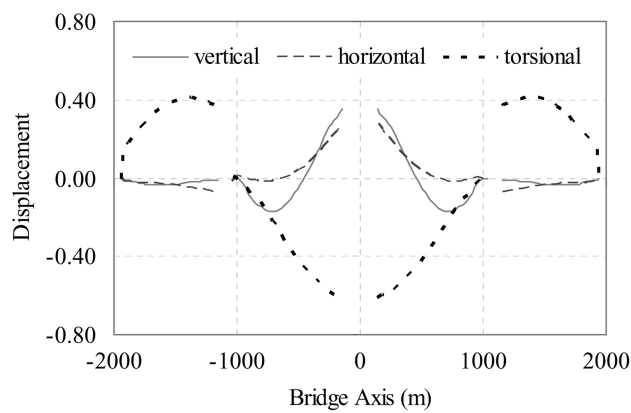Fig. 18 Flutter mode shape at 85% deck completion by midspan-to-pylon configuration

Fig. 19 Flutter mode shape at 85% deck completion by pylon-to-midspan configuration

6.3. Effects of single TMD and multi TMD on flutter response during erection

Effects of single TMD in each mode and multi TMD on aerodynamic response are investigated. Single TMD in each mode and multi TMD with 1% and 2% mass ratio by midspan-to-pylon

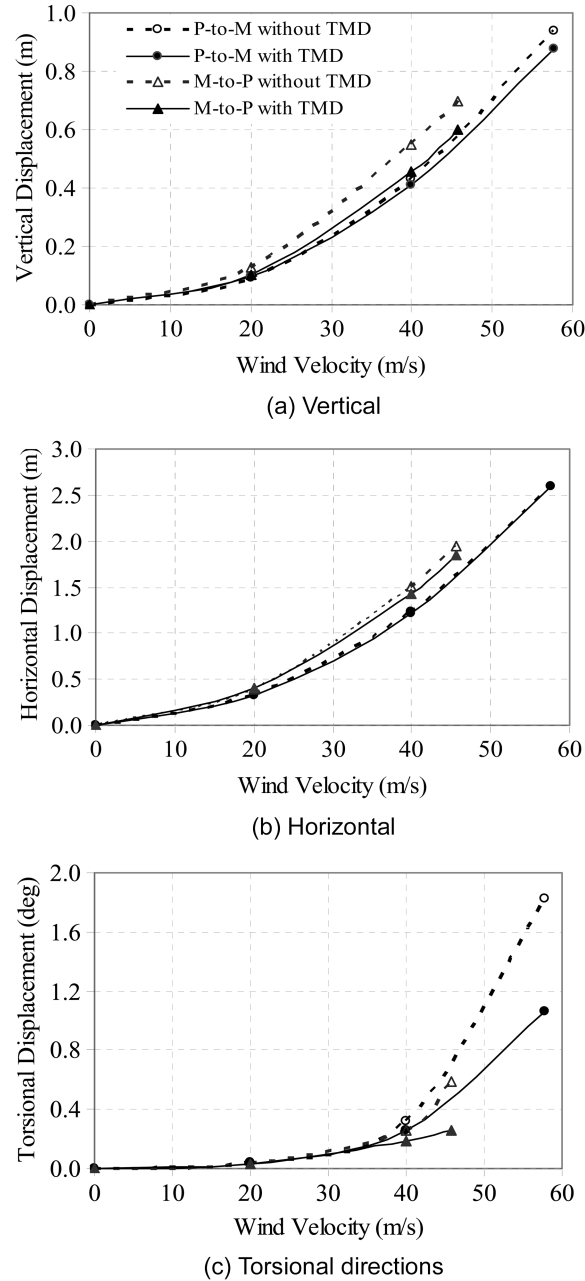(a) Vertical

(b) Horizontal

(c) Torsional directions

Fig. 20 Comparisons of std displacement response at 85% deck completion with and without TMD type1 at end of deck by pylons-to-midspan and at the center node of the main span by midspan-to-pylons

configuration and pylon-to-midspan configuration are considered. The results show that, similar to the completed bridge case, the single TMD in each mode and multi TMD result in no significant change in the critical wind velocity for flutter instability. For example, the single TMD tuned to T1 mode, and multi TMD tuned to H1, V1, and T1 modes lead to a slight increase in the critical wind velocity for flutter instability. Therefore, the detailed results are not shown here.

6.4. Effects of multi TMD on buffeting response during erection

The multi TMD type 1 consists of the vertical and horizontal TMD with 1% mass ratio in each direction together with a torsional TMD with ratio of 1% mass moment of inertia of the bridge during erection is investigated. The multi TMD type 1 is installed at the span-center section for midspan-to-pylon configuration and at the two end sections for pylon-to-midspan configuration. Comparisons of std displacement response at 85% deck completion with and without multi TMD type 1 at the center node of the main span by midspan-to-pylons configuration and at end of deck by pylon-to-midspan configuration are shown in Fig. 20. The results show that, similar to the completed bridge case, when velocity increases, the control efficiency of multi TMD in reducing the torsional buffeting response increases greatly. However, its control efficiency in the vertical and horizontal directions reduces.

7. Conclusions

The suppression of aerodynamic response of long-span suspension bridges during erection and after completion by using single TMD and multi TMD is presented in this paper. An advanced finite-element-based aerodynamic model that can be used to analyze both flutter instability and buffeting response in the time domain is also proposed. The modal damping of a structure-TMD system is analyzed by the state-space approach. From the numerical examples of the Akashi Kaikyo Bridge, the conclusions are summarized as follows:

When the wind velocity is low, about 20 m/s, the multi TMD type 1 (the vertical and horizontal TMD with 1% mass ratio in each direction together with a torsional TMD with ratio of 1% mass moment of inertia) can significantly reduce the buffeting response in terms of the std value in vertical, horizontal and torsional directions by 8.6-13%.

When the wind velocity increases to 40 m/s, the control efficiency of multi TMD type 1 in reducing the torsional buffeting response increases greatly to 28% because the torsional aerodynamic damping reduces with the wind velocity. However, its control efficiency in vertical and horizontal directions reduces because the aerodynamic dampings in these directions increase with the wind velocity and become more dominant than TMD.

The single TMD and multi TMD result in no significant change in the critical wind velocity for flutter instability. This is because the rate of increase of negative aerodynamic damping is so high when the wind velocity approaches the flutter velocity.

The control efficiency of TMD in reducing the torsional buffeting response increases greatly as the ratio of the mass moment of inertia of TMD increases from 1% to 3% at high wind velocity. Although, its control efficiency in vertical and horizontal directions tends to saturate or even decrease as the mass ratio of TMD increases from 1% to 3%, its mass ratio in vertical and horizontal directions may increase up to 2-3% for the long-span bridge to reduce the peak stroke of TMD and to make its stroke move within the operation range inside the stiffening truss girder.

The critical wind velocity for flutter instability during erection is significantly lower than that for the completed bridge. The critical wind velocity during erection by pylon-to-midspan configuration is significantly higher than that by midspan-to-pylon configuration. By midspan-to-pylon configuration, the minimum critical wind velocity of 41.20 m/s occurs at an early stage of about 25-40% deck completion. By pylon-to-midspan configuration, the minimum critical wind velocity of 57.70 m/s occurs at the stage of 85% deck completion.

Similar to the completed bridge case, when velocity increases, the control efficiency of multi TMD in reducing the torsional buffeting response of bridge during erection increases greatly. However, its control efficiency in vertical and horizontal directions reduces.

Acknowledgements

References

Agar, T. J. A. (1991), "Dynamic instability of suspension bridges", *Comput. Struct.*, **41**(6), 1321-1328.
Ayorinde, E. O. and Warburton, G. B. (1980), "Minimizing structural vibrations with absorbers", *J. Earthquake Eng. Struct. Dynamics*, **8**, 219-236.
Boonyapinyo, V., Miyata, T. and Yamada, H. (1999), "Advanced aerodynamic analysis of suspension bridges by state-space approach", *J. Struct. Eng.,* ASCE, **125**(12), 1357-1366.
Brancaleoni, F. (1992), "The construction phase and its aerodynamic issues", *Aerodynamics of Larger Bridges*, Larsen, A. Ed., Balkema, Rotterdam, The Netherlands, 147-158.
Change, C. C., Gu, M. and Tang, K. H. (2003), "Tuned mass dampers for dual-mode buffeting control of bridges", *J. Bridge Eng.*, ASCE, **8**(4), 237-240.
Chen, X., Matsumoto, M. and Kareem, A. (2000a), "Aeodynamic coupling effects on flutter and buffeting of bridges" *J. Eng. Mech.*, ASCE, **126**(1), 17-26.
Chen, X., Matsumoto, M. and Kareem, A. (2000b), "Time domain flutter and buffeting response analysis of bridges", *J. Eng. Mech.*, ASCE, **126**(1), 7-16.
Cobo del Arco, D. and Aparicio, A. (2001), "Improving the wind stability of suspension bridges during construction", *J. Struct. Eng.*, ASCE, **127**(8), 869-875.
Conti, E., Grillaud, J., Jacob, J. and Cohen, N. (1996), "Wind effects on normandie cable-stayed bridge: comparison between full aeroelastic model test and quasi-steady analytical approach", *J. Wind Eng. Ind. Aerodyn.*, **65**, 189-201.
Fujino, Y., Wilde, K., Masukawa, J. and Bhartia, B. (1995), "Rational function approximation of aerodynamics forces on bridge deck and its application to active control of flutter", *Proc. 9th Int. Conf. on Wind Engineering*, New Delhi, India, 994-1005.
Ge, Y. J. and Tanaka H. (2000), "Aerodynamic stability of long-span suspension bridges under erection", *J. Struct.*, ASCE, **126**(12), 1404-1412.
Gimsing N. J. (1997), *Cable Supported Bridges: Concept & Design*, 2nd Ed., John Wiley & Sons, New York.
Gu, M., Chang, C. C., Wu, W. and Xiang, H. F. (1998), "Increase of critical flutter wind speed of long-span bridges using tuned mass dampers", *J. Wind Eng. Ind. Aerodyn.*, **73**, 111-123.
Gu, M., Chen, S. R. and Chang (2001), "Parametric study on multiple tuned mass dampers for buffeting control of yangpu bridge", *J. Wind Eng. Ind. Aerodyn.*, **89**, 987-1000.
Honshu-Shikoku Bridge Authority (1995), "Full-bridge-model wind-tunnel experiment of Akashi Kaikyo

Bridge", *Annual Report 1995*, Tokyo, Japan (in Japanese).

Kwon, S.-D. and Park K.-S. (2004), "Suppression of bridge flutter using tuned mass dampers based on robust performance design", *J. Wind Eng. Ind. Aerodyn.*, **92**, 919-934.

Larsen, A. and Gimsing, N. J. (1992), "Wind engineering aspects of the east bridge tender project", *J. Wind Eng. Ind. Aerodyn.*, **42**, 1405-1416.

Malhortra, L. and Wieland, M. (1987), "Tuned mass damper for suppressing wind effects in cable-stayed bridges", *Proc. Int. Conf. on Cable-Stayed Bridges*, Bangkok.

Miyata, T., Sato, H. and Kitagawa, M. (1993), "Design consideration for superstructures of the Akashi Kaikyo bridge", *Proc. Int. Seminar on Utilization of Large Boundary Layer Wind Tunnel*, Tsukuba, Japan, 121-139.

Miyata, T. and Yamada, H. (1988), "Coupled flutter estimate of a suspension bridge", *J. Wind Eng.*, Japan, **37**, 485-492.

Miyata, T., Yamada, H., Boonyapinyo, V. and Santos, J. C. (1995), "Analytical investigation on the response of a very long suspension bridge under gusty wind", *Proc. 9th Int. Conf. on Wind Engineering*, New Delhi, India, 1006-1017.

Nobuto, J., Fujino, Y. and Ito, M. (1988), "A study on the effectiveness of TMD to suppress a coupled flutter of bridge deck", *Proc. of the Japan Society of Civil Engineering*, No. 398/I-10, pp. 413-416.

Pourzeynali, S. and Datta, T. K. (2002), "Control of flutter of suspension bridge deck using TMD", *Int. J. Wind Struct.*, **5**(5), 407-422.

Samaras, E., Shinozuka, M. and Tsurui, A. (1985), "ARMA representation of random process", *J. Eng. Mech.*, ASCE, **111**(3), 449-461.

Scanlan, R. H. (1988), "On flutter and buffeting mechanisms in long-span bridges", *Probabilistic Eng. Mech.*, **3**(1), 22-27.

Simiu, E. and Scanlan, R. H. (1996), *Wind Effects on Structures*, 3rd Ed., John Wiley & Sons, New York, N.Y.

Tanaka, H., Larose, G. L. and Kimura, K. (1992), "Aerodynamics of long-span bridges during erection", *Aerodynamics of Larger Bridges*, Larsen, A. Ed., Balkema, Rotterdam, The Netherlands, 119-127.

Waldlaw, R. L. (1992), "The improvement of aerodynamic performance", *Aerodynamics of Larger Bridges*, Larsen, A. Ed., Balkema, Rotterdam, The Netherlands, pp. 59-70.

Wilde, K. and Fujino, Y. (1998), "Aerodynamic control of bridge deck flutter by active surfaces", *J. Eng. Mech.*, ASCE, **124**(7), 718-727.

CC